



Effect of CO₂ injection on heterogeneously permeable coalbed reservoirs



Hemant Kumar^{a,*}, Derek Elsworth^a, Jonathan P. Mathews^a, Jishan Liu^b, Denis Pone^c

^aJohn and Willie Leone Family Department of Energy and Mineral Engineering, EMS Energy Institute and G³ Center, Pennsylvania State University, University Park, PA 16802, USA

^bSchool of Mechanical and Chemical Engineering, The University of Western Australia, WA 6009, Australia

^cConocoPhillips, Houston, TX, USA

HIGHLIGHTS

- The recovery is rapid at higher CO₂ injection pressures.
- However, CO₂ breakthrough occurs earlier at higher injection pressures.
- The homogenizing influence of CO₂-swelling is outpaced by CH₄-shrinkage.
- This leaves the reservoir open to short-circuiting and earlier breakthrough.
- The cumulative CO₂ produced and stored is proportional to the injection pressure.

ARTICLE INFO

Article history:

Received 14 January 2014

Received in revised form 30 June 2014

Accepted 2 July 2014

Available online 16 July 2014

Keywords:

Coalbed

Permeability

Numerical modeling

Heterogeneous

ECBM

ABSTRACT

Enhanced coalbed methane (ECBM) can be recovered by injecting a gas such as carbon dioxide into the reservoir to displace methane. The contrast between density, viscosity, and permeability of the resident and displacing fluids affects the efficiency of ECBM recovery. The prediction of earlier breakthrough becomes complex as the permeability may vary by orders of magnitude during gas injection and methane recovery. Predominantly, the reservoir permeability is modulated by the pore pressure of the sorptive gas (CH₄ and CO₂) and effective stresses. Here we explore the possibility of early breakthrough and its implications for managing coalbed reservoirs during CO₂ assisted ECBM. A coupled finite element (FE) model of binary gas flow, diffusion, competitive sorption and permeability change is used to explore the effect of CO₂ injection on net recovery, permeability evolution and injectivity in uniform and homogeneously permeable reservoirs. This effect is evaluated in terms of dimensionless pressure (p_D), permeability (k_D) and fracture spacing (x_D) on the recovery of methane and permeability evolution for ECBM and non-ECBM scenarios. We have considered two scenarios (4 MPa and 8 MPa) of constant pressure injection of CO₂ for ECBM. The increase in production rate of CH₄ is proportional to k_D but inversely proportional to x_D .

Further, a reservoir with initial permeability heterogeneity was considered to explore the effect of CO₂ injection on the evolution of permeability heterogeneity – whether heterogeneity increases or decreases. The evolution of permeability heterogeneity is investigated for the same two CO₂ injection scenarios. For the specific parameters selected, the model results demonstrate that: (1) The injection of CO₂ in coalbed reservoirs increases the production nearly 10-fold. (2) At higher injection pressures the recovery is rapid and the production increases dramatically – the production increases 2-fold on increasing the CO₂ injection pressure from 4 MPa to 8 MPa. (3) However, CO₂ breakthrough occurs earlier at higher injection pressures. (4) The permeability heterogeneity in the reservoir is reduced after a threshold time (~500 days) although the overall heterogeneity is increased relative to the initial condition and is overall increased for both non-CO₂ and CO₂ injection scenarios. This indicates that the homogenizing influence of CO₂-sorption-swelling is outpaced by CH₄-desorption-shrinkage and effective stress influences. This leaves the reservoir open to short-circuiting and earlier breakthrough of CO₂ rather than having this effect damped-out by the homogenizing influence of swelling. (5) The cumulative volume of CO₂ produced and stored in the reservoir is proportional to the injection pressure.

© 2014 Elsevier Ltd. All rights reserved.

* Corresponding author. Present address: Chevron-ETC, Houston, TX, USA.

E-mail address: Hemant.Kumar@Chevron.com (H. Kumar).

1. Introduction

Enhanced coalbed methane (ECBM) recovery may be promoted by the injection of carbon dioxide as CO₂-ECBM. The lower physorption affinity of CH₄ in coal promotes its desorption on injection of CO₂ in coal seams [1,2]. The enhanced recovery of CH₄ with injection of CO₂ can be as high as 90% as compared to conventional pressure depletion methods (50%) [3]. There is potential for CO₂ sequestration in deep unminable coal seams ranging from 6% to 20% of the total sequestration capacity worldwide [3].

Coalbed reservoirs are self-sourcing with the majority of the CH₄ stored in the adsorbed state in the coal matrix [4]. Some laboratory investigations for pure gas adsorption on pulverized coal indicated that the adsorption of CO₂ on a molar basis may be approximately two times that of CH₄ in American bituminous coals [5]. The volumetric adsorption capacity ratio of CO₂/CH₄ on coal ranges from one on anthracite coal to ten for low-rank coals [3]. This ratio may be larger at higher pressures for all ranks coal [6,7]. The permeability of coalbed reservoirs is principally determined by the fracture network (cleats) while the coal matrix is considered relatively impermeable [8]. The cleat permeability is controlled by the dynamic effective stress regime and by the adsorption/desorption induced swelling/shrinkage of the matrix during continued production [9–13]. Gas adsorption and related swelling is influenced by sorption capacity, coal rank, maceral composition and the composition of the permeating gas [10,14–16]. The dynamics of swelling/shrinkage becomes more complex if the coalbed methane production is assisted by CO₂ injection. The presence of sorptive gases (CH₄ and CO₂) swells the matrix resulting in reduction of cleat aperture while desorption promotes cleat dilation for constrained coals under in situ conditions. CO₂-injection for ECBM often results in net swelling of the coal matrix [12,14,16–19] and the additional matrix strain will reduce the fracture aperture leading to porosity and permeability loss [20,21]. The competitive adsorption, sorption capacity, matrix shrinkage/swelling and permeability transformations are among the important factors affecting CO₂ assisted ECBM. With continuous production of methane from a bituminous coal, the permeability increases one-hundred fold and the rate of increase accelerates [22]. The displacement of CH₄ with CO₂ injection in laboratory experiments causes significant changes in the stress/strain fields [23] and decreases the permeability which is partly attributed to swelling. There have been many experimental studies exploring the effect of coal rank [24,25], maceral composition [25], moisture content [26], sorption [27] and in situ stress on the strain dilation [12,15,28], stiffness [29], porosity loss [8], permeability transformations [10,26], sorption capacity [23,30,31] and transport characteristics.

There are multiple demonstration sites around the world exploring both CBM and ECBM. The Allison unit in the San Juan basin (US), for example explored CO₂-ECBM. The CH₄ production data on CO₂ injection in coal seams indicated various phenomena e.g. matrix shrinkage/swelling leading to permeability enhancement/loss [32]. Up to a one-hundred fold increase in permeability was observed in some wells [32–34]. Reservoir simulation studies for production forecast and history matching have been conducted for various CBM and ECBM fields [34–37]. Various models have been proposed to predict these permeability transformations [8,14,36,38–49]. An existing single well for CO₂-ECBM micro-pilot test in anthracite coals of South Qinshui basin, Shanxi Province, China was successfully simulated for the production of CH₄ [50]. ECBM recovery and CO₂ storage in Appalachian thin seams was simulated for horizontal wells and it was recommended that the mixture of flue gas and CO₂ would yield better recovery than the pure CO₂ injection [36]. The observations from a CO₂-ECBM test

project in a 6 m thick coal seam at Yubari, Northern Japan were found to be consistent with CO₂ sorption induced swelling in coal [51].

These observations from experimental, pilot plant, and simulation studies may be exploited for optimizing CO₂-ECBM recovery. The model implemented here includes the dynamics of gas flow, diffusion, competitive sorption and permeability change to explore the effect of CO₂ injection on net recovery, permeability evolution, and injectivity in a homogeneous reservoir. The cleats in the coal have a wide range of apertures therefore the permeability of the fractures may vary over a similarly wide range. To explore and quantify permeability evolution under such practical constraints we extended our FE model to examine the impact of permeability heterogeneity.

2. This study

The objective of this study is to develop a dual porosity FE model for binary gases (CH₄ and CO₂) where coal matrix and fractures are represented by dual continua. This model may be used for explicitly quantifying the interactions between the binary gases and sorbing solid media during CO₂ assisted ECBM recovery. We have implemented a general porosity model for matrix and fractures together with a general permeability model for the matrix. A new model for fracture permeability, under conditions of in situ stress and constrained displacement has been implemented [10]. The FE model implemented here presents insights into the non-linear response of CH₄ depletion, CO₂ injection, porosity transformation, permeability evolution for the matrix and fracture system during continued production of CH₄ with concomitant injection of CO₂. A logical sequence of this model extends to a model which has initial fracture permeability heterogeneity in the coalbed reservoir. This FE model assumes a Gaussian normal distribution of permeability at the beginning of the production and predicts the change in permeability during the life span of the reservoir. The behavior of the CO₂-ECBM system is governed by a set of field equations consisting of coal deformation, multi-gas adsorption, and gas transport. These equations are coupled with porosity and permeability transformations in both matrix and fractures within an FE solver. We have made some assumptions to allow the solving of these highly non-linear constitutive and field equations simultaneously.

2.1. Assumptions

The coal is conceptualized as component solid blocks (coal matrix) attached together with springs as fractures, as shown in Fig. 1. Here fracture spacing and fracture aperture are referred to

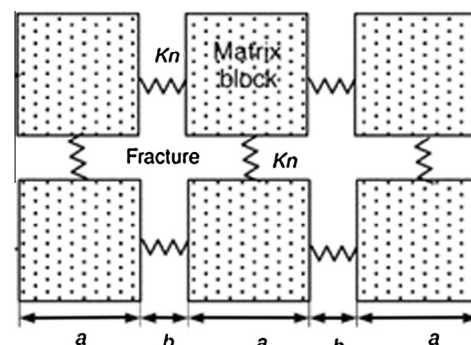


Fig. 1. Schematic representation of coal-fracture dual continuum system [35].

as a and b respectively. More details may be found in previous publications [10,35,39,52,53].

The following assumptions were implemented for the development of the FE simulator.

- (1) The CBM reservoir consists of a dual elastic continuum representing matrix and fracture. They are homogeneous, isotropic and isothermal.
- (2) The water in the reservoir is immobile and the gas flow obeys Darcy's Law for a single phase.
- (3) The gas present in the pores of the reservoir is ideal and its viscosity is a function of pressure but not temperature as the reservoir is isothermal.
- (4) A zero strain condition exists in the reservoir.

2.2. Field equations

2.2.1. Binary gas adsorption

A coalbed methane reservoir often contains more than 80% CH₄, together with a mixture of other higher hydrocarbons and CO₂ [54]. This study assumes that the CBM reservoir contains primarily CH₄ (85%) and minor amounts of CO₂ (15%). This gas mixture governs the reservoir characteristics. The remaining gas components are ignored. The equation of state for an ideal gas holds the following relation between pressure, volume and temperature in both matrix and fractures (Eq. (1))

$$pV = nRT \quad (1)$$

If the concentration C is represented as number of moles per unit volume, $C = \frac{n}{V}$ then Eq. (1) can be rewritten as,

$$p = CRT \quad (2)$$

where p [Pa] is pressure, V [m³] is volume, R [m³ Pa/K/mol] is gas constant, n is number of moles, T [K] is temperature.

The gas adsorbed in the coal matrix follows the Langmuir sorption relation and the gas volume adsorbed per unit of coal mass can be calculated using the Langmuir equation [55] as given in Eq. (3)

$$V = \frac{V_L p_m}{p_m + p_L} \quad (3)$$

where V_L is the adsorbed volume per unit of coal at infinite pressure, p_m is the equilibrium pressure of gas in the matrix, p_L is the Langmuir pressure and V is the volume adsorbed per unit of coal mass at pressure p_m .

The adsorption of two (binary) or more than two gases in an adsorbent may be expressed by the Extended Langmuir Isotherm (ELI) as follows (Eq. (4)):

$$V_k = \frac{V_{k0} C_k b'_k}{1 + \sum_{j=1}^N C_j b'_j} \quad (4)$$

where V_{k0} is the adsorbed volume of pure species per unit of coal at infinite pressure, C_k is the equilibrium concentration of gas in the matrix, b'_k is $1/(p_L \cdot R \cdot T)$ and V is the volume adsorbed per unit of coal mass at concentration c_m for species k . Similarly, the contribution of an individual species in an n -species mixture towards sorption induced volumetric strain may be expressed as [35]

$$\varepsilon_k = \varepsilon_{Lk} \frac{C_k b'_k}{1 + \sum_{j=1}^n C_j b'_j} \quad (5)$$

The total sorption induced strain can be calculated by summing the strain caused by each species as, [35]

$$\varepsilon_s = \sum_{k=1}^n \varepsilon_k = \sum_{k=1}^n \varepsilon_{Lk} \frac{C_k b'_k}{1 + \sum_{j=1}^n C_j b'_j} \quad (6)$$

where ε_{Lk} is the strain developed by a pure species at infinite pressure, ε_k is the strain developed at concentration of gas C_k in the matrix for species k and ε_s is the total strain developed by all species in the coal. Note that $k = 1$ and 2 are for CH₄ and CO₂ respectively in the formulation.

2.2.2. Binary gas transport

Typically a CBM reservoir is partially dewatered first to produce gas. The onset of water removal occurs when the seam pore pressure is below a critical pressure usually corresponding to saturation pressure [10]. The pressure depletion in the reservoir triggers various transport process on different length scales. These are:

(1) The primary porosity system *i.e.* coal matrix where the permeability is negligible and the diffusion (majorly Fickian) is the dominant mode of flow. (2) The secondary porosity system, *i.e.* face or butt cleat system (fractures), where the flow is laminar and obeys Darcy law. (3) Transfer of mass between matrix and fractures where the matrix may act as both source or sink depending upon the pressure head. The mass balance equation implemented here is based on the premise that gas is flowing under the simultaneous influence of a pressure field (Darcy's Law) and a concentration field (Fick's Law), therefore the velocities are additive [56].

A detailed analysis may be found in previous publications [35,52]. The mass balance equation incorporating the above mentioned convective, diffusive and transfer flux flow may be expressed as,

$$\frac{\partial m_k}{\partial t} + \nabla \cdot (\vec{v} \cdot \rho_{gk}) + \nabla \cdot (-D_k \cdot \nabla m_{kf}) = Q_{sk} \quad (7)$$

where the gas content of a component gas k is m_k which includes both free-phase and adsorbed gas. The mass of each component of gas present in a unit of the coal-matrix and fracture system can be written as,

$$\text{For fracture, } m_{fk} = \phi_f \cdot C_{fk} \cdot M_{fk} \quad (8)$$

$$\text{For matrix, } m_{mk} = \phi_m \cdot C_{mk} \cdot M_{mk} + (1 - \phi_{m0}) \cdot \rho_c \cdot \rho_{sg} \cdot \frac{V_{Lk} b'_k C_{mk}}{1 + C_{m1} b'_1 + C_{m2} b'_2} \quad (9)$$

The convective velocity \vec{v} is determined by the concentration gradient in the fracture or matrix and can be expressed as,

$$\vec{v}_f = -\frac{k_f RT}{\mu} \nabla C_{fk} \quad (10)$$

$$\vec{v}_m = -\frac{k_m RT}{\mu} \nabla C_{mk} \quad (11)$$

where ρ_{gk} is the gas density, ρ_{sg} is the gas density at standard conditions, ρ_c is the coal density, M_k is the molar mass of component k , Q_{sk} is the gas source or sink, and Q_k is the hydrodynamic dispersion coefficient defined as Eqs. (12) and (13),

$$D_{fk} = \beta_c \cdot \vec{v}_f + D_{fk0} \quad (12)$$

$$D_{mk} = \beta_c \cdot \vec{v}_m + D_{mk0} \quad (13)$$

where D_{k0} is the coefficient of molecular diffusion of component k and β_c is the dynamic dispersivity.

The transfer flux ω_k between matrix and fracture for a component of gas k may be written as [57]

$$\omega_k = -\frac{3\Pi^2}{a^2} \quad (14)$$

where a is the fracture spacing in a cube block model [58].

2.3. Constitutive equation

2.3.1. Porosity model for matrix and fracture

The porosity for the coal matrix can be defined [35,38,40,50,59] as a function of single gas adsorption,

$$\varphi_m = \varphi_{m0} - \frac{\alpha}{K} \frac{1}{\frac{b_0}{aK_f} + \frac{1}{K}} \left(\frac{\varepsilon_L P_m}{P_L + P_m} - \varepsilon_v \right) \quad (15)$$

where φ_{m0} is the initial matrix porosity, α is the Biot coefficient for the coal matrix, K is the matrix bulk modulus, K_f is the modified fracture stiffness, $K_n = K_f/b_0$ is the fracture stiffness, b_0 is the initial fracture aperture and φ_m is the matrix porosity.

If the sorption is caused by a binary mixture of gases then the volumetric strain term in Eq. (15) can be replaced by Eq. (6) and the matrix porosity equation yields,

$$\varphi_m = \varphi_{m0} - \frac{\alpha}{K} \frac{1}{\frac{b_0}{aK_f} + \frac{1}{K}} \left(\sum_{k=1}^2 \varepsilon_{Lk} \frac{C_{mk} b'_k}{1 + \sum_{j=1}^n C_{mj} b'_j} - \varepsilon_v \right) \quad (16)$$

Similarly, the porosity of the fracture system can be expressed as [35]

$$\frac{\varphi_f}{\varphi_{f0}} = 1 + \frac{\Delta b}{b_0} = 1 - \frac{3}{\varphi_{f0} + \frac{3K_f}{K}} \left(\sum_{k=1}^2 \varepsilon_{Lk} \frac{C_{mk} b'_k}{1 + \sum_{j=1}^n C_{mj} b'_j} - \varepsilon_v \right) \quad (17)$$

where φ_{f0} is the initial fracture porosity, Δb is the differential change in aperture and φ_f is the fracture porosity. The subscript f and m are for fracture and matrix respectively in each parameter.

2.3.2. Permeability model for matrix and fracture

The permeability of the matrix can be expressed as [35],

$$\frac{k_m}{k_{m0}} = \left(1 - \frac{\alpha}{\varphi_{m0} K} \frac{1}{\frac{b_0}{aK_f} + \frac{1}{K}} \left(\sum_{k=1}^2 \varepsilon_{Lk} \frac{C_{mk} b'_k}{1 + \sum_{j=1}^n C_{mj} b'_j} - \varepsilon_v \right) \right)^3 \quad (18)$$

where k_{m0} is the initial matrix permeability and k_m is the permeability of matrix.

Based on our previous work [10] the permeability of the fracture network in coal may be expressed as a function of gas pressure, effective stress and moisture content as,

$$\frac{k_{fk}}{k_{f0k}} = \left\{ \left(1 + \frac{C_k p_{mk}}{p_{mk} + P_{Lk}} \right)^3 + e^{-\beta_k \sigma'} \right\} * e^{-\delta_k S_w} \quad (19)$$

where k_{f0} is the initial permeability of the fracture system, p_m is the gas pressure in the matrix, p_L is the Langmuir pressure constant, σ' is effective stress, S_w is the moisture content of the coal and k_f is the permeability of the fracture system. The fitting parameters are C , β and δ in this model. Note that subscript $k = 1$ or 2 is for CH_4 and CO_2 respectively.

3. Analysis of permeability

3.1. Flow instability in CO_2 sweep

In the context of ECBM recovery, a high viscosity fluid (CO_2) displaces a low viscosity fluid, *i.e.* interstitial CH_4 . The high viscosity fluid CO_2 exhibits lower permeability than CH_4 at the same pore pressure under similar confining conditions [10]. The possible flow instability is investigated using the Saffman–Taylor instability criterion [60]. The velocity of the displacing and displaced fluid is assumed to be the same on either side of the sweeping front. The perturbations grow with time in an unstable front. This can be formulated as follows after ignoring the gravitational effects.

$$\left(\frac{\left(\frac{\mu_1 \varphi_1}{k_1} - \frac{\mu_2 \varphi_2}{k_2} \right) U}{\left(\frac{\mu_1 \varphi_1}{k_1} + \frac{\mu_2 \varphi_2}{k_2} \right)} \right) \geq 0 \quad (20)$$

Here μ_1 , μ_2 are viscosities, φ_1 , φ_2 are porosities and k_1 , k_2 are permeabilities for CH_4 and CO_2 respectively. The velocity of the sweeping front is represented by U .

If the porosity is assumed to be equal on both side of the sweeping front then Eq. (20) may be rewritten as,

$$\frac{k_1}{k_2} \leq \frac{\mu_1}{\mu_2} \quad (21)$$

The maximum viscosity ratio for CH_4 and CO_2 is $\sim 3/4$. However the permeability ratio on the left hand side of the Eq. (21) is more than 1 at any given pore pressure for both gases. This indicates that the sweeping front is unconditionally stable and the amplitude of perturbations would dampen leading to a stable sweeping front.

3.2. Dimensionless analysis

In a unit volume of fracture, the mass of the species and its rate of change is the net result of advection of the species into the volume which is governed by Darcy flow $\nabla \cdot \left(-\frac{k_f}{\mu} p_f \nabla \cdot p_f \right)$ and addition or removal of the species from the volume due to exchange with the matrix $\pm \frac{3\Pi^2}{a^2} \frac{k_m}{\mu} p_f (p_f - p_m)$. The mass balance of the unit volume is defined as

$$[\varphi_f] \frac{\partial p_f}{\partial t} + \nabla \cdot \left(-\frac{k_f}{\mu} p_f \nabla \cdot p_f \right) = -\frac{3\Pi^2}{a^2} \frac{k_m}{\mu} p_f (p_f - p_m) \quad (22)$$

Eq. (22) can be rearranged as

$$\frac{1}{p_f} [\varphi_f] \frac{\partial p_f}{\partial t} + \nabla \cdot \left(-\frac{k_f}{\mu} \nabla \cdot p_f \right) = -\frac{3\Pi^2}{a^2} \frac{k_m}{\mu} (p_f - p_m) \quad (23)$$

Dividing Eq. (23) by p_m , k_m/μ and $1/a^2$ the resulting form may be expressed as

$$\frac{\mu a^2}{k_m p_f p_m} [\varphi_f] \frac{\partial p_f}{\partial t} - a^2 \frac{k_f}{k_m} \nabla \cdot \left(\nabla \cdot \frac{p_f}{p_m} \right) = 3\Pi^2 \left(1 - \frac{p_f}{p_m} \right) \quad (24)$$

For simplicity the one dimensional form may be written as

$$\frac{\mu a^2}{k_m p_f} [\varphi_f] \frac{\partial (p_f/p_m)}{\partial t} - \frac{k_f}{k_m} \frac{\partial}{\partial (x/a)^2} \left(\frac{p_f}{p_m} \right) = 3\Pi^2 \left(1 - \frac{p_f}{p_m} \right) \quad (25)$$

The dimensionless variables in Eq. (25) are pressure p_D , permeability k_D , characteristic length x_D and time t_D . They can be expressed as

$$p_D = \left(\frac{p_f}{p_m} \right); \quad k_D = \left(\frac{k_f}{k_m} \right); \quad x_D = \left(\frac{x}{a} \right); \quad t_D = \frac{t}{\frac{\mu a^2}{k_m p_f}}$$

The dimensionless form of the mass conservation relation can be written as

$$\varphi_f \frac{\partial p_D}{\partial t_D} - k_D \frac{\partial p_D}{\partial x_D^2} = 3\Pi^2 (1 - p_D) \quad (26)$$

Eq. (26) indicates that the dimensionless pressure, permeability, and characteristic length may play an important role in the production of CH_4 . This has been investigated by varying p_D , k_D and x_D parameters in the later sections.

4. Model implementation

The physics implemented in this study simulates the behavior of CO_2 assisted ECBM. The case presented here simulates a dewatered coalbed reservoir so the production of water is not

considered. We use a five well pattern where an injection well (IW) lies at the center of a square array of four production wells (PW) as shown in Fig. 2. A similar configuration has been used in the past for ECBM multi well pilot testing [61] and has been simulated using various approaches [35,62]. The configuration presented here is a proxy of a five well pattern deployed in a ECBM field in the South Qinshui Basin, Shanxi, China [61]. All the wells are assumed to be vertical.

We have utilized conservation of mass for each gas together with flux transfer between matrix and fracture depending on the pressure difference. The exchange of gases (CH₄ and CO₂) under the phenomenon of adsorption/desorption, governed by the extended Langmuir isotherm, triggers transformations in porosity and permeability in the matrix-fracture system. The transformations in porosity and permeability affect the flow of fluid in the fracture network which is governed by Darcy's law. Darcy and diffusion driven flow are implemented in the matrix however, diffusion is the dominant transport mode. The CH₄ residing in the matrix is released as the gas pressure reduces and results in matrix-shrinkage. The fracture network receives the released CH₄. With the continued production of CH₄ and injection of CO₂, the permeability changes with time due to matrix shrinkage/swelling effects. Presumably, a higher rate of CO₂ injection would staunch the reservoir permeability quickly and the permeability drop-rate would be higher.

Also, permeability heterogeneities are employed in the model with mean permeability defining behavior indexed to that of the homogeneous system. The range of the permeability varies from very low (same as that of matrix) to very high (equal to one Darcy). This allows us to investigate the effect of CO₂ injection on the evolving heterogeneity of the reservoir.

4.1. Model description

For the sake of simplicity only a one-quarter section, as outlined with the red dotted line in Fig. 2, is simulated. This one-quarter section of the reservoir is represented by a two dimensional block of sides 160 m × 160 m (Fig. 3). The lower left corner has a one-quarter section of the CO₂ injection well (IW) and the upper right corner of the geometry has a one-quarter section of a CH₄ production well (PW), (Fig. 3). The diameter of the wells is assumed to be 0.1 m. The model has no flow conditions for all the boundaries except the well boundaries where a constant pressure condition has been assumed at the well boundaries. It was also assumed that the production well produces at 0.1 MPa or 1 atm bottom-hole pressure. We have considered three scenarios of CO₂ injection: namely no injection, and injection at pressures of 4 MPa and 8 MPa, respectively. The initial pore pressures of CH₄ and CO₂ in

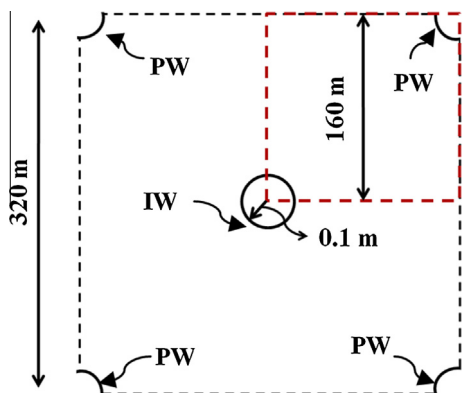


Fig. 2. A typical five well patterns with four production wells (PW) and one injection well (IW) at the center.

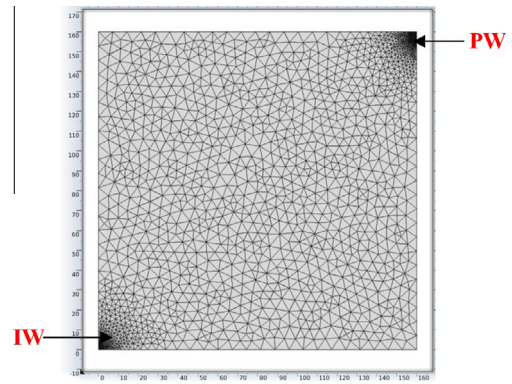


Fig. 3. Schematic of a one-quarter section (shown with red dotted boundary in Fig. 2) of a five-well pattern. The grid has been laid over the geometry using COMSOL Multiphysics.

the reservoir have been assumed as 3.0 MPa and 0.5 MPa, respectively.

All boundaries of the simulated area are fixed. The unique values of the properties used in this model are taken from the literature [35] and are presented in Table 1. The total simulation time was for 30 years (~10⁹ s). The model has been implemented in an adaptive mesh mode for fluid dynamics. All the results obtained in this study are independent of mesh size and time step. The model was benchmarked with our previous studies [35,52].

4.2. Homogeneous system

The initial permeability of the fracture network is assumed homogeneous i.e. all the mesh elements in the reservoir have the same permeability at time zero. Unique values of the properties used in this section are presented in Table 1. As the CBM reservoir starts producing with or without the injection of CO₂ the permeability of the reservoir changes. The total production, the transformation of concentration ratio (CH₄/CO₂) and the rate of production are investigated for varying injection pressures, fracture-matrix permeability ratios, and fracture spacing under three scenarios of CO₂ injection. These injection scenarios are those of no injection, and injection at 4 MPa and 8 MPa discussed earlier.

4.2.1. Effect of injection pressure

The total cumulative production from the CBM reservoir in 30 years is shown in Fig. 4a under three scenarios. It is clear from

Table 1 The values of modeling parameters used in simulations [10,35,63].

Symbol	Parameter	Value	Unit
E	Young's Modulus of coal	2.71	GPa
E_S	Young's Modulus of coal grain	8.13	GPa
N	Poisson's ratio of coal	0.34	-
ρ_c	Density of coal	1.25×10^3	kg/m ³
μ_{CH_4}	CH ₄ dynamic viscosity	1.15×10^{-5}	Pa s
μ_{CO_2}	CO ₂ dynamic viscosity	1.60×10^{-5}	Pa s
P_{L,CH_4}	CH ₄ Langmuir pressure constant	2.07	MPa
P_{L,CO_2}	CO ₂ Langmuir pressure constant	1.38	MPa
V_{L,CH_4}	CH ₄ Langmuir volume constant	0.0256	m ³ /kg
V_{L,CO_2}	CO ₂ Langmuir volume constant	0.0477	m ³ /kg
ϵ_{L,CH_4}	CH ₄ Langmuir volumetric strain constant	0.0128	-
ϵ_{L,CO_2}	CO ₂ Langmuir volumetric strain constant	0.0237	-
ϕ_{m0}	Initial porosity of matrix	0.0423	-
ϕ_{f0}	Initial porosity of fracture	0.001	-
k_{m0}	Initial permeability of matrix	3.0×10^{-17}	m ²
k_{f0}	Initial permeability of fracture	3.0×10^{-15}	m ²
a	Fracture spacing	0.01	m
b	Average aperture of the fracture	1×10^{-3}	m

Figs. 4a and 4b that the injection of CO₂ at 8 MPa yields the highest cumulative production ($2.5 \times 10^5 \text{ m}^3$) with the maximum rate of recovery (peak rate $175 \text{ m}^3/\text{day}$) in ~ 30 years. Also, a spectacular increase in the rate of production is observed in the case of CO₂ injection as compared to no injection. The rate of production decreases almost exponentially with injection pressure. The highest production rate occurs with 8 MPa injection while no injection yields the minimum production rate (Fig. 4b). It is important to note that the “no-injection” scenario yields significantly less production in ~ 30 years than that of the 8 MPa injection case ($\sim 1/10$ th). It indicates that the injection of CO₂ increases the net CH₄ production. These simulation results are in agreement with previous findings for homogeneous reservoirs [35,36]. The injection of CO₂ however is expected to reduce the permeability and therefore the injectivity. It was suspected that the injection of CO₂ may hinder CH₄ production due to coal swelling, however, the opposite trends has been observed in Alberta during multi well pilot testing [64]. The permeability increase/decrease is dictated by the ‘U-shaped’ permeability evolution [10]. Thus it is important where the initial reservoir pressure sits on this “U-shaped” permeability–pressure relation. Fig. 5, shows the permeability evolution in the matrix and fractures for the three scenarios considered. The injection of CO₂ at 8 MPa and the no-injection scenarios exhibit the highest and lowest fracture permeability respectively in a period of ~ 30 years. Note that the average fracture permeability changes as the pore pressure modulates due to injection or production after time $t = 0$. If the observation from CH₄ production and permeability evolution are combined it is apparent that injection at 8 MPa yields the highest production with a maximum permeability, while injection at 4 MPa yields three fold less production as compared to the 8 MPa injection but two fold more than no injection. The permeability in the 4 MPa injection case was between that for the 8 MPa and no injection cases during the life of the reservoir. For the no-injection scenario, the fracture permeability peaks at ~ 500 days and then declines due to increased CO₂ mole fraction in the reservoir with ongoing production. These observations indicate that the reservoir yields the lowest production with minimum injectivity in the no injection case, therefore the CO₂-ECBM approach is useful for this reservoir.

The surface map of methane mole fraction in the matrix (Fig. 6) indicates that the CH₄ content decreases faster with CO₂ injection than with no injection. However, the velocity of the sweeping front is approximately twice faster in the 8 MPa injection than for the 4 MPa injection. For instance, at the end of 100 days, the CO₂ front reaches only 20 m from the injection well bore for the 4 MPa injection case but 40 m when injection was carried out at 8 MPa (Fig. 6).

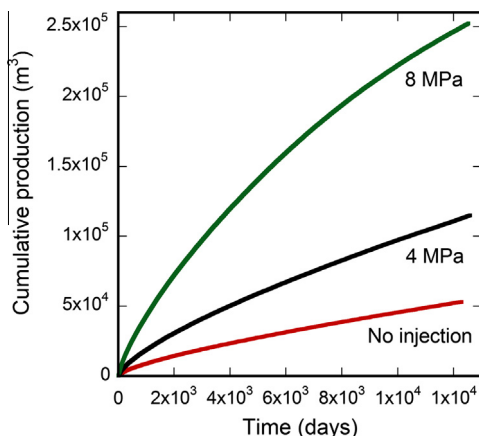


Fig. 4a. Total cumulative production of CH₄ for constant pressure CO₂ injection (4 MPa and 8 MPa) and no CO₂ injection scenarios.

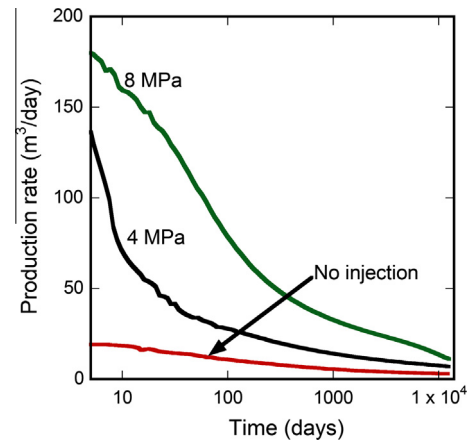


Fig. 4b. Rate of production of CH₄ for two CO₂ injection (8 MPa and 4 MPa) and the one no CO₂ injection scenarios.

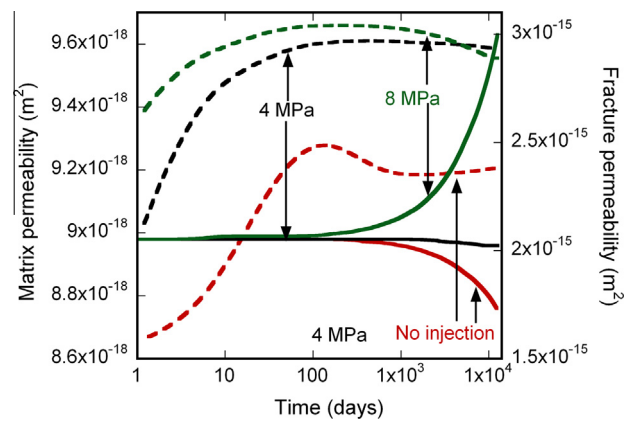


Fig. 5. The average permeability of the matrix and fracture for no injection, 4 MPa injection and 8 MPa injection scenarios. The solid and dashed lines represent matrix and fracture permeability respectively.

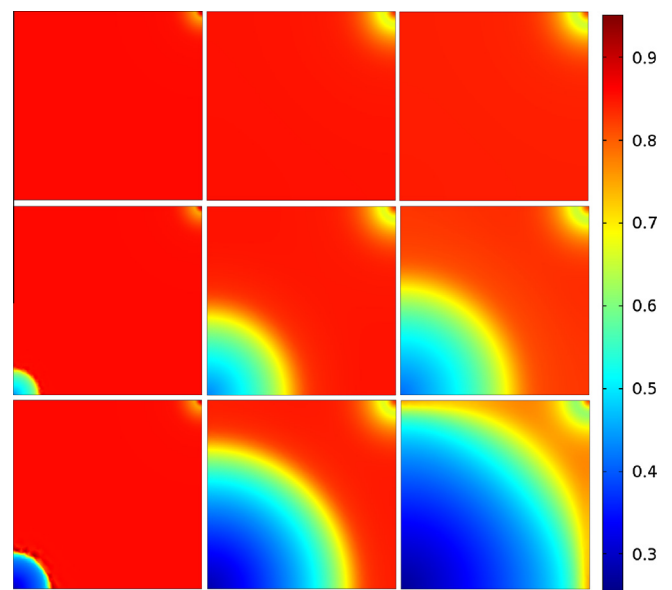


Fig. 6. The distribution of methane mole fraction for no injection, 4 MPa injection and 8 MPa injection scenarios (from top to bottom) at various times 100, 3000 and 7000 days (from right to left) in the matrix. The low and high color represents the value of 0.25 and 0.95 respectively. (For interpretation of the references to color in this figure legend, the reader is referred to the web version of this article.)

Thus, higher injection pressures yield a greater swept area in a given time. The ratio of average concentration ratio of the two gases CH₄ and CO₂ in the reservoir may also indicate the efficiency and rate of sweep. The concentration ratio of CH₄:CO₂ decreases faster in both matrix and fracture for 8 MPa versus 4 MPa and is faster for 4 MPa than for the no-injection scenario (8 MPa > 4 MPa > no-injection; Fig. 7) indicating faster and more effective recovery of methane from the reservoir for the higher the pressure. These trends are similar to the field observations in various CO₂-ECBM fields [65,66].

4.2.2. Effect of fracture matrix permeability ratio

Based on the dimensionless analysis (Eq. (26)) it is clear that the dimensionless permeability $k_d = k_f/k_m$ may have a significant effect on the total gas production and rate of production. The dimensionless permeability is varied by varying the k_{f0}/k_{m0} ratio as 1, 10, 100 for no injection, 4 MPa and 8 MPa injection. The dimensionless permeability remains almost constant for 10–100 days depending upon the initial value. The rise in k_d occurs earlier for higher values of k_d compared to lower values. The fracture permeability increases and the matrix permeability remains approximately the same therefore the dimensionless permeability shows slight increase until 100 days as shown in Fig. 8b for $k_d = 100$. The dashed lines in Fig. 8 shows the evolution of k_d at the center of the block mid-way between wells (point A: (80,80)). The evolution of k_d at point A approximately represents the k_d for the entire reservoir for the particular cases discussed here at the values of the properties given in Table 1. This may not hold true for other configurations not discussed in this paper. At later times (1000–10,000 days), k_d becomes almost constant indicating that the relative change in the permeability of matrix and fracture is close to steady state. It is interesting to note that the permeability evolution in these three cases have different characteristics with gradual changes until ~30 years.

Fig. 9a and b, shows the evolution of permeability of matrix and fracture for two scenarios of CO₂ injection (4 MPa and 8 MPa) along the cut section (IW) for various times. The matrix permeability decreases from injection well to production well in the 4 MPa and 8 MPa injection cases. As the matrix exchanges CH₄ with the injected CO₂ the permeability of the matrix increases (Fig. 9a and b). The permeability of the matrix is higher near the injection well as compared to the area near the production well. Permeability is reduced at the production well due to matrix shrinkage accompanying CH₄ and CO₂ desorption in the vicinity of the production wellbore. The rate of change of permeability change in the matrix

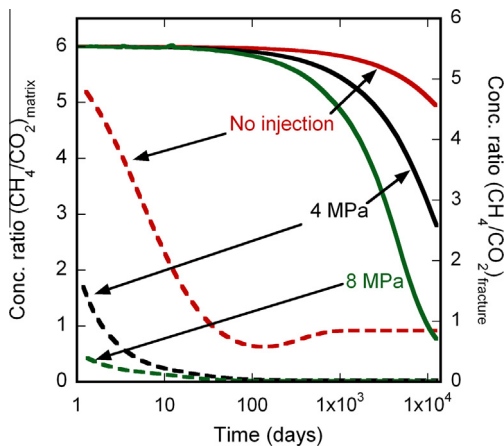


Fig. 7. The evolution of the ratio of average concentration of CH₄ and CO₂ in the matrix (solid lines) and fracture (dashed lines) for no injection, 4 MPa injection and 8 MPa injection scenarios at various time steps.

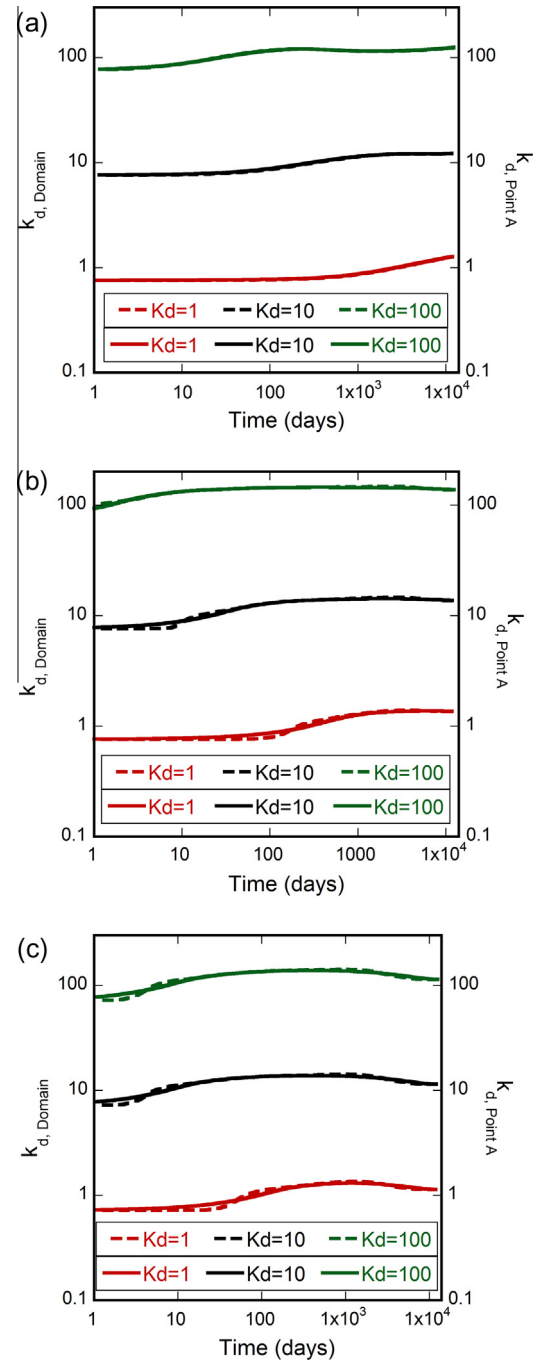


Fig. 8. The evolution of dimensionless permeability (k_d) with time for (a) no injection, (b) 4 MPa injection and (c) 8 MPa injection (top to bottom). The solid lines represent the mean value of (k_d) for the entire reservoir and dashed lines show the value for a point A (80,80).

is faster for 8 MPa injection compared to the 4 MPa injection case. The permeability change front moved only 100 m away from the injection well in ~10 years in the case of 4 MPa injection while it has travelled 150 m for injection at 8 MPa.

The fracture permeability evolution was more dramatic than the permeability transformations in the matrix. The change in matrix permeability is as high as ~10% while the change in fracture permeability may vary by ~200%. The fracture permeability is principally governed by the concentration of sorptive gases, their mole fractions and effective stresses [10]. To a large extent, the fracture permeability increases away from the injection wellbore

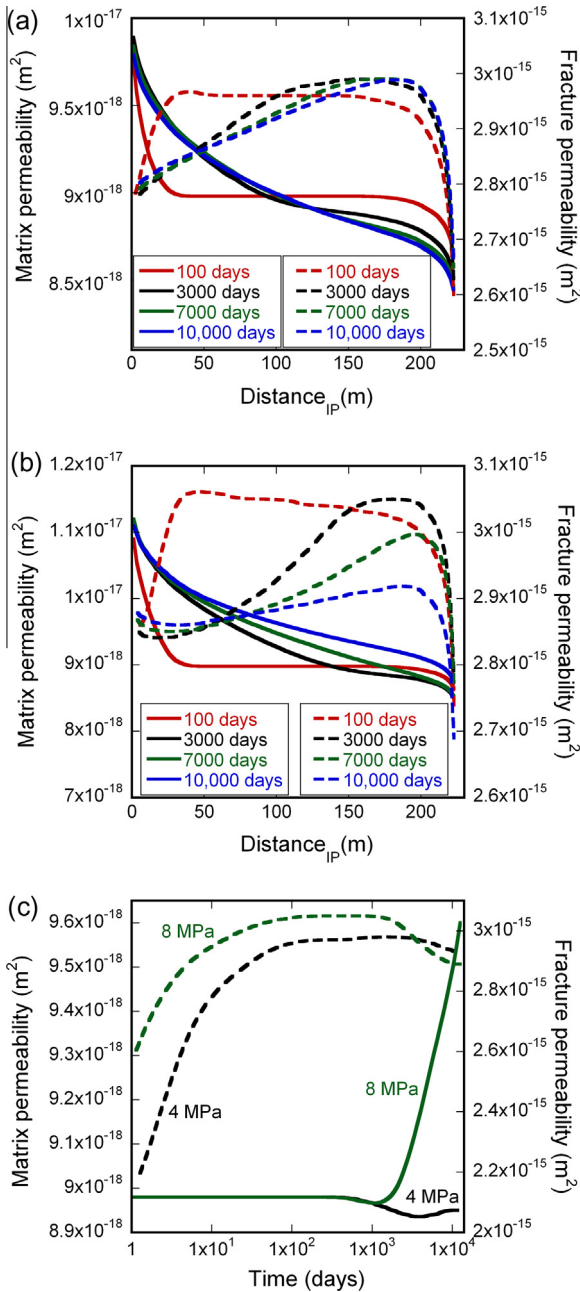


Fig. 9. The matrix and fracture permeability along a cut section (IW) for injection at (a) 4 MPa, (b) 8 MPa and (c) evolution of matrix and fracture permeability at point A (80,80) for 4 MPa and 8 MPa injection at various time steps. The solid lines show the matrix permeability and the dashed lines represent matrix permeability at various times.

and achieves a maximum value and then decreases on approaching the production wellbore. However the fracture permeability observations are slightly different for each scenario of CO₂ injection considered for this study. For instance, the permeability decreases away from the injection wellbore until ~10 m and then increases reaching a limiting value followed by a drop towards the production well bore in the case of 8 MPa injection. The CO₂ affected permeability zone travels from 50 m (100 days) to 150 m (>10 years) in the case of 4 MPa injection while it reaches to 200 m in the same time frame if the CO₂ is injected at 8 MPa. As the matrix adsorbs more gas it expands and the porosity of the matrix increases slightly and therefore the permeability is enhanced but the matrix swelling decreases the fracture

permeability by occupying the fracture space reducing the fracture permeability. However, the fracture permeability evolution is influenced by additional parameters too.

Fig. 9c, shows the permeability evolution in matrix and fracture at point A (80,80), which is equidistant from injection and production wells, for 4 MPa and 8 MPa injection scenarios. The matrix permeability remains unaffected for ~100 days and then decreases for 10 years. The permeability of matrix was regained as the matrix adsorbs injected CO₂. The permeability of the matrix at the end of 30 years is higher than its initial value in the case of 8 MPa injection however the gain in permeability with CO₂ injection at 4 MPa is less as it merely recovers to its initial value. The fracture permeability at point A (equidistant from the injection and production wells) increases with time, reaching a plateau in ~3 years and then decreases until ~30 years. This behavior is attributed to shrinkage caused by production at earlier times followed by swelling due to enhanced sorption of CO₂ occurring later. It is important to note that the matrix and fracture permeability evolve in opposite directions but by different multipliers. If the matrix permeability increases at a point then the fracture permeability competitively decreases and vice versa.

4.2.3. Effect of fracture spacing

The dimensionless analysis of Eq. (26) indicates that the dimensionless length $x_D = a/L$ is another parameter which may play a significant role on production. The value of the parameter L is fixed for the five well pattern configurations. Three scenarios of dimensionless length are simulated corresponding to fracture spacing a as 0.01, 0.02 and 0.04 m for CO₂ injection at 4 MPa. These represent the spacing of fractures at meter-scale rather than at cleat scale. The injection of CO₂ at 4 MPa may allow slow removal of CH₄ as it is only 0.5 MPa higher than the initial reservoir pressure. The production rate is higher in the case of the smallest fracture spacing (Fig. 10) which can be attributed to the reduced diffusive length for sorption/desorption. Relatively small diffusive lengths allow more gas to flow into the fractures and the flow in the fracture is faster than the diffusive flow in the matrix. Therefore, the diffusive length acts as a rate determining parameter for the production. The cumulative production also increases marginally with decreasing fracture spacing (not shown). The ratio of concentrations of CH₄ to CO₂ decays faster with smaller values of fracture spacing (Fig. 11a). As the diffusive lengths are small the exchange of CO₂ with CH₄ is faster allowing a quicker CH₄ recovery. The concentration ratio drops rapidly within fractures as compared to the matrix. The CH₄ present in the fracture is recovered almost instantaneously (~10 days) at the start of CO₂ injection. More gas is

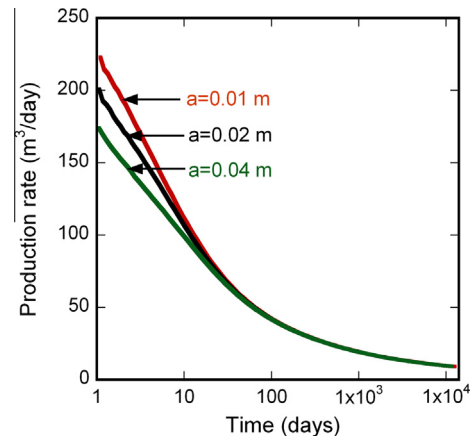


Fig. 10. The rate of production with varying fracture spacing on constant pressure injection of CO₂ at 4 MPa.

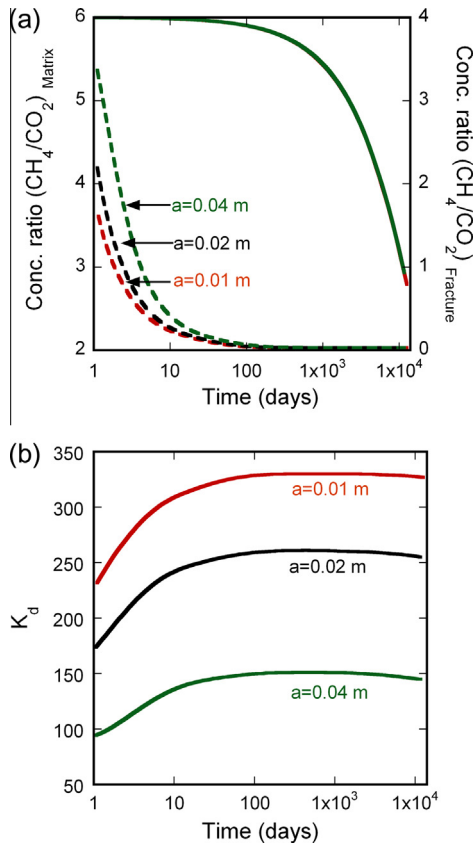


Fig. 11. (a) The ratio of average concentration of CH₄ and CO₂ in the matrix at various time steps. The solid lines show the concentration ratio in matrix and the dashed lines represent the concentration ratio in fractures. (b) The evolution of average dimensionless permeability with time.

removed from the matrix due to an increased concentration gradient after removal of free CH₄ from the fractures and this process accelerates when the coal matrix exchanges CH₄ with injected CO₂.

The evolution of dimensionless permeability with fracture spacing is investigated for the 4 MPa injection case (Fig. 11b). The change in dimensionless permeability *k_d* increases by 40–60% of its initial values in ~30 years depending on the initial fracture spacing (Fig. 11b). The change in the values of dimensionless permeability indicates that the fractures achieve significantly higher values of permeability in comparison to matrix as the depletion proceeds. The highest change observed (~60%) for *k_d* was for the longest fracture spacing (*a* = 0.04 m) as the highest volume shrinkage occurs for the longest fracture spacing. The volume shrinkage assists the fracture to accommodate more fluid to flow in the Darcy regime.

4.3. Heterogeneous system

The natural fracture network of a coalbed reservoir offers a wide range of spatial variation in permeability due to the variation in the fracture apertures from one location to another. This spatial distribution of permeability is referred to as permeability heterogeneity. To the best of our knowledge, previous models developed for CO₂-ECBM have not included consideration of the effects permeability heterogeneity. This methodology allows a more realistic representation of coalbed reservoirs produced under CO₂-ECBM. To achieve this the permeability is distributed in the geometry as a Gaussian normal distribution such that the average permeability remains identical to that of a homogeneous configuration and the permeability values range from a maximum (10⁻¹³ m²) to a

minimum (10⁻¹⁸ m²). All other parameters assume the unique values presented in Table 1. The heterogeneity in permeability is shown in Fig. 12 and is accommodated by coupling with binary gas adsorption, binary gas transport, porosity transformations and permeability evolution in the matrix and fracture as a dual continuum present in the reservoir. The reservoir is simulated to investigate the effect of CO₂ injection on the reinforcing or ameliorating influences of permeability heterogeneity on the permeability evolution of the matrix and fractures, on earlier breakthrough and CO₂ and of CO₂ storage under various scenarios of CO₂ injection.

4.3.1. Effect on heterogeneity

The initial permeability heterogeneity may increase or decrease with the progress of injection for various CO₂ injection scenarios. This is explored using a heterogeneous permeability configuration with specified mean and standard deviation. If the standard deviation of the total observations is small then permeability heterogeneity is small. For example, if the standard deviation of permeability decreases then the reservoir attains more uniform permeability configuration. Fig. 13a, shows the evolution of average fracture permeability and standard deviation of the permeability for various scenarios of CO₂ injection. The production of methane induces matrix shrinkage in the reservoir and the average fracture permeability increases for a year and then decreases (~5 years) followed by a permeability plateau after 20 years under no injection (Fig. 13a). The drop in permeability for 1–5 years is due to increased mole fraction of CO₂ due to pressure driven depletion. The permeability for ECBM scenarios (4 MPa and 8 MPa) increases for the earlier times achieving a maximum in ~100 days then decreases as the concentration of CO₂ increased in the reservoir. The decrease in permeability at later times (>20 years) is due to exchange of CH₄ with more sorptive CO₂.

The evolution of the standard deviation of the permeability for the no injection scenario suggests that the reservoir shifts towards a more heterogeneous permeability configuration with continued production (Fig. 13a and b). The matrix surrounded by high permeability fractures desorbs faster compared to the matrix surrounded by low permeability fractures. The CH₄ desorption results in matrix shrinkage and fracture aperture enhancements. Which further accelerates the preferential desorption from high permeability areas. In this process, the larger aperture fractures tend to increase in aperture at a faster rate than smaller aperture fractures, resulting in more heterogeneous distribution of permeability. There is an increase in standard deviation of permeability followed by reduction in its values for the 4 MPa and 8 MPa CO₂ injection cases. The increase in standard deviation may be attributed to matrix

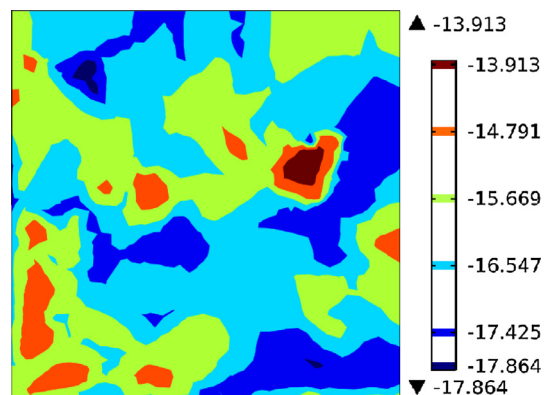


Fig. 12. The fracture permeability in the reservoir varies from 10⁻¹³ to 10⁻¹⁸ m². The variation assumes a Gaussian normal distribution with a mean as 10⁻¹⁵ m².

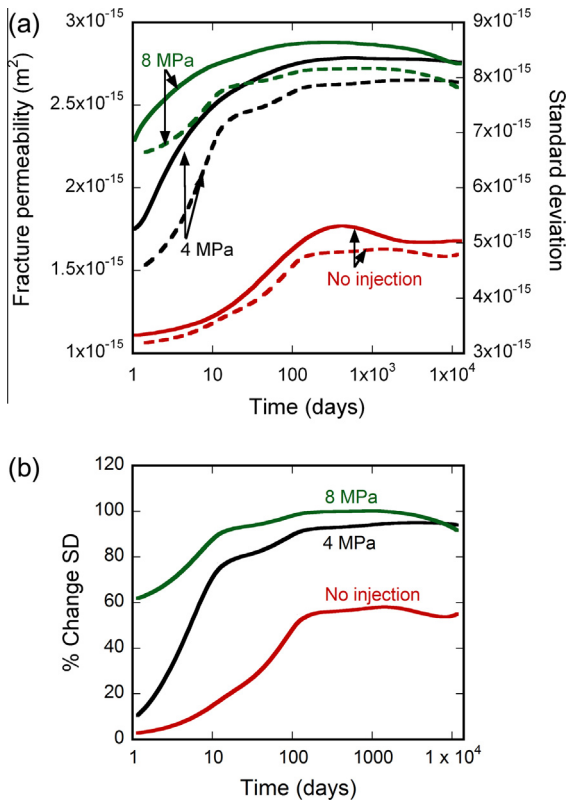


Fig. 13. (a) The mean and standard deviation of permeability in the reservoir at various times. The injection of CO_2 has been considered for 4 MPa and 8 MPa pressure. The no-injection scenario is also shown. The solid and dashed lines indicate fracture permeability and standard deviation respectively. (b) The percentage change in standard deviation of permeability in the reservoir domain.

shrinkage at earlier times followed by matrix swelling due to enhanced sorption of injected CO_2 . The decrease in standard deviation indicates that the permeability heterogeneity reduces with time and the reservoir achieves a more homogenous configuration under ECBM approaches. A practical implication is that the CO_2 flows through the largest aperture fractures first inducing swelling in the nearby matrix which results in reduction of the fracture apertures. The reduction in permeability of the larger aperture fractures diverts the fluid through the other higher permeability fractures. We expect a selective flow mechanism where CO_2 flow finds a path of least resistance (higher permeability) in the reservoir and when the resistance increases with time it diverts the fluid to the lower resistance path. This process helps the reservoir to achieve more homogeneous permeability configuration as indicated by changes in the standard deviation of permeability (Fig. 13b). The standard deviation of permeability plateaus ~ 500 days and then decreases till ~ 30 years (Fig. 13b) indicating the reservoir reaches homogeneous permeability configuration as time proceeds. The surface distribution of fracture permeability with time is shown in Fig. 14. The permeability heterogeneity (contrast in colors) disappears relatively faster with 8 MPa injection (Fig. 14).

4.3.2. Effect on fracture and matrix permeability

The evolution of permeability in matrix and fracture is investigated for the reservoir with initial permeability heterogeneity. Fig. 15, shows the evolution of average matrix and fracture permeability for no injection, 4 MPa and 8 MPa injection scenarios. The permeability evolution show similar trend as observed before for homogeneous permeability (Fig. 15). The permeability of the

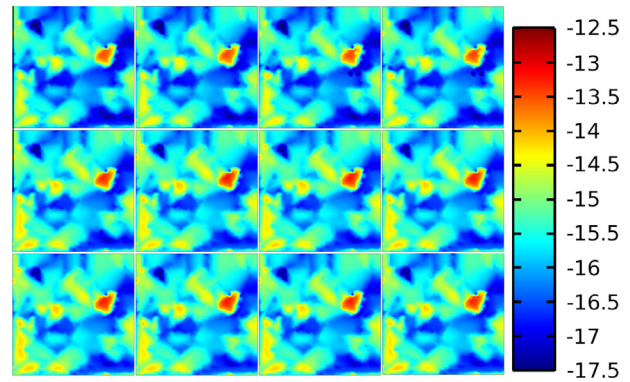


Fig. 14. The surface map of fracture permeability at various time steps from left to right (100, 3000, 7000 and 10,000 days) for no injection, 4 MPa and 8 MPa CO_2 injection scenarios from top to bottom. Cold colors represent less permeable areas in the reservoir. The color scale on right side represents the permeability (m^2) in the exponent of 10. (For interpretation of the references to color in this figure legend, the reader is referred to the web version of this article.)

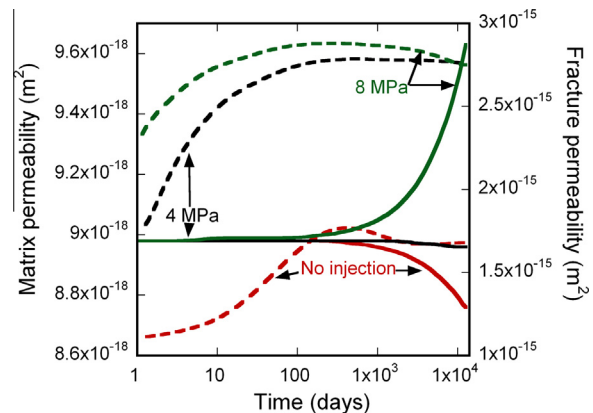


Fig. 15. The evolution of permeability in matrix and fracture in the domain. The permeability value represents the average for the entire reservoir. The solid and dashed lines indicate matrix permeability and fracture permeability respectively.

fracture increases for all scenarios in the beginning and then drops as the sorption of injected CO_2 occurs. The concentration of CO_2 and CH_4 in the matrix is plotted across the diagonal section linking IW to PW for the reservoir for the three cases considered for the study for various times (Fig. 16). The concentration profile in all three cases is smooth despite the initial heterogeneity in fracture permeability. This indicates the innate stability of the sweeping CO_2 front even within a reservoir containing permeability heterogeneity. Pockets of high concentration are observed at earlier times in areas (fracture only) with initial low permeability (not shown). However, the concentration in these pockets reduces with time. The reduction of CH_4 concentration and increase of CO_2 concentration increases with injection pressure (Fig. 16b and c). As time proceeds, the concentration of CO_2 increases in the reservoir and the concentration profile along the cut section becomes steeper with time (Fig. 16).

4.3.3. Effect on breakthrough

Enhanced production for CBM reservoirs is observed with CO_2 injection. However a significant fraction of injecting fluid (CO_2) will also be recovered in the production wells before recovering the majority of the interstitial fluid (CH_4) referred. This is known as 'breakthrough'. We investigate the breakthrough for the heterogeneous distribution of permeability under no injection and two CO_2 injection scenarios. The evolution of average concentration ratio

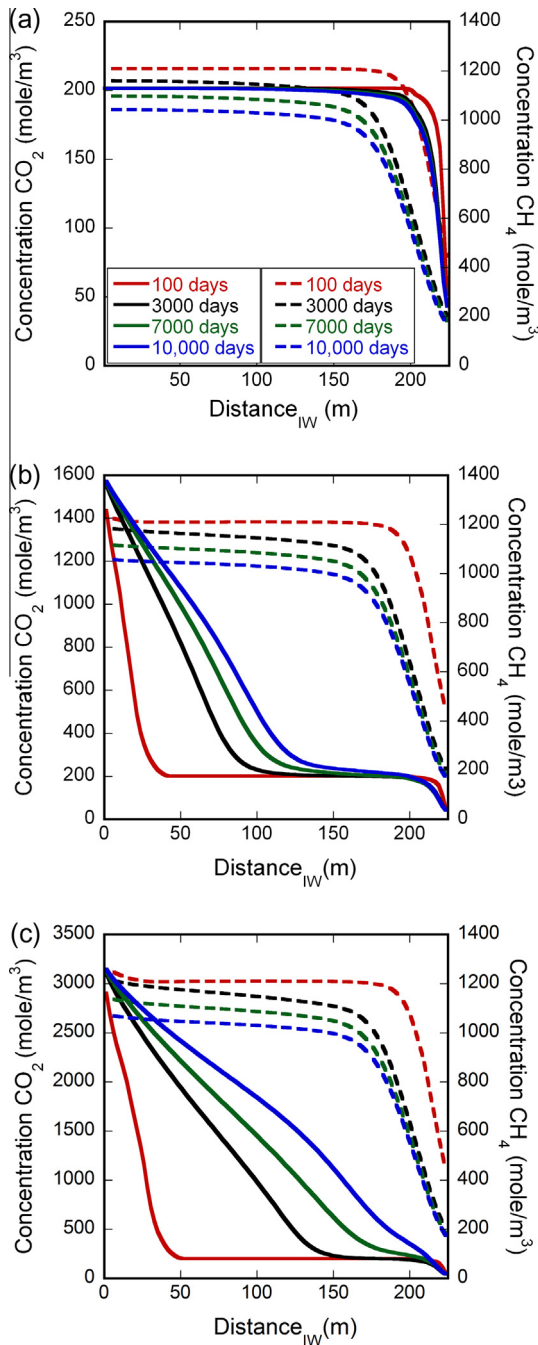


Fig. 16. The variation in concentration of CH₄ and CO₂ along the diagonal (IW-PW) at various time steps. (a) No injection (top left), (b) 4 MPa injection (top right) and (c) 8 MPa injection (bottom). The time legends are shown in (a). The solid and dashed lines indicate CO₂ and CH₄ concentrations respectively.

(CH₄/CO₂) in the fracture and matrix is shown in Fig. 17. The concentration ratio drops rapidly in the fractures (~10–100 days) compared to the matrix where this process might take ~25 years. The injection pressure affects both the fracture permeability and therefore the quantity of injected CO₂ volume in the reservoir. Therefore, injection pressure affects the rate of the concentration reduction in the fractures (Fig. 17). Among the three cases, the fracture permeability is highest with 8 MPa CO₂ injection (Fig. 15) hence the movement of injecting fluid (CO₂) is faster in this case which promotes the faster removal of residing fluid (CH₄) in the fracture. This fast removal of CH₄ from the system results in the sharp decline of concentration ratio (Fig. 17). Presumably, faster removal of CH₄ triggers the matrix to release more gas into the

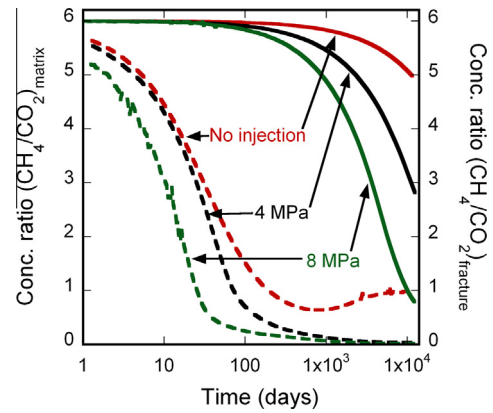


Fig. 17. Evolution of the average of concentration ratio (CH₄ and CO₂) in the reservoir with time. A sharp decline from one value to another shows displacement without mixing flow. The solid and dashed lines indicate the concentration ratio (CH₄:CO₂) in the matrix and fracture respectively.

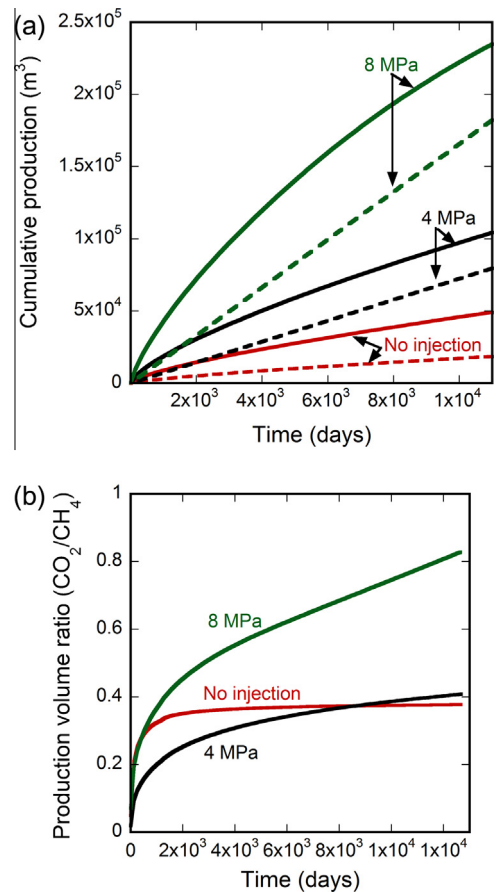


Fig. 18. (a) The cumulative production of CH₄ and CO₂ over time and (b) the volume ratio of CO₂/CH₄ in the production well for no-injection, 4 MPa and 8 MPa injections. The solid and dashed lines indicate cumulative production of CH₄ and CO₂ respectively in (a).

fracture network to equilibrate the concentration in fracture. The released CH₄ is removed by CO₂ and the system keeps removing increasingly more and more CH₄ with the help of injected CO₂. The injection of CO₂ at higher pressure (8 MPa) increases the total recovery (Fig. 18a) and the rate of production but it also increases the CO₂ production (Fig. 18a). The elevated rates of recovery of CO₂ from the production well follow the order 8 MPa > 4 MPa > No Injection. It is important to note that the CH₄ and CO₂ may be

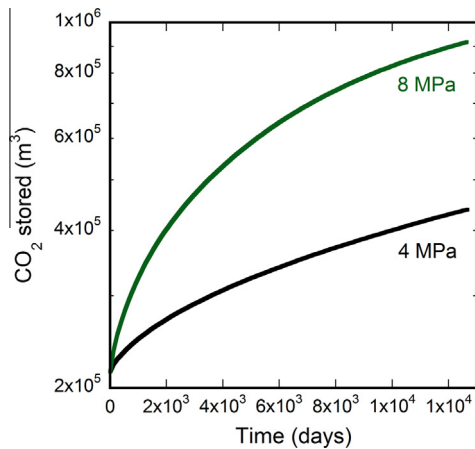


Fig. 19. The cumulative volume of CO₂ sequestered by injection of CO₂ at 4 MPa and 8 MPa over ~30 years.

separated at the well-head and the CO₂ may be re-injected. The relative expense of separation of the CO₂ is relevant to the overall economic viability of ECBM production.

The mole fraction of production on a volume basis is shown in Fig. 18b. Here, breakthrough is defined as the time when the production stream contains a majority of injected fluid. This happens when the mole fraction of CO₂ is 0.5 or the ratio of their produced volumes is 1. Fig. 18, indicates that the 8 MPa injection scenario approaches the earlier breakthrough faster as compared to 4 MPa and no-injection scenario. The volumetric ratio of CO₂ and CH₄ in the production stream is highest when CO₂ is injected at 8 MPa, indicating that the production stream contains a significant amount of CO₂ in comparison to the 4 MPa or no-injection scenarios. The observations from total production of CH₄ and CO₂ and their volumetric ratio do not rationalize the preference of one scenario over the others. However, it is clear that the maximum production of CH₄ could be achieved only with 8 MPa injection though it would also yield higher CO₂ production leading to higher separation costs.

4.3.4. Effect on CO₂ storage

The CO₂ assisted ECBM may also be utilized for CO₂ sequestration. The injected CO₂ is partly stored in the reservoir and a fraction of it is recovered with the CH₄ production. Fig. 19, shows the cumulative CO₂ stored in the reservoir in ~30 years. The net CO₂ stored in the reservoir increases with time for both 4 MPa and 8 MPa CO₂ injections. The volume of CO₂ stored in the reservoir at 8 MPa injection is double that stored for injection at 4 MPa.

The majority of CO₂ in the coalbed reservoirs are in the adsorbed state in the coal-matrix. The stored CO₂ increases with injection pressure (Fig. 19). Congruent with the Langmuir isotherm (Eq. (4)) the adsorbed mass of gas in the matrix increases with gas pressure leading to enhanced storage of CO₂ in the coalbed at higher injection pressures.

5. Conclusions

In this work, the interactions between binary gas mixtures (CO₂ and CH₄) and dual solid media (coal matrix and fracture) are simulated using a commercially available finite element (FE) solver. The FE solver is utilized to implement various models into a coupled simulator. The implemented model includes binary gas flow, diffusion, competitive sorption and permeability change to explore the effect of CO₂ injection on net recovery, permeability evolution and injectivity in uniform or homogeneous permeability reservoirs. Dimensionless parameters (pressure p_D , permeability k_D

and spacings x_D) are derived and their effect on permeability evolution is explored for CBM (no CO₂-injection) and CO₂-ECBM (4 MPa and 8 MPa) injection scenarios. Further, a reservoir with initial permeability heterogeneity is considered to explore the effect of CO₂ injection on the evolution of permeability heterogeneity – whether heterogeneity increases or decreases. The results indicate the complexity of the interaction of coal matrix-fracture systems with dual sorptive gases CH₄ and CO₂. However, some general observations and conclusions of this study are:

- (1) The injection of CO₂ in coalbed reservoirs increases the production of CH₄ nearly 10-fold.
- (2) At higher injection pressures the recovery is rapid and the production increases dramatically – the production increases 2-fold on increasing the CO₂ injection pressure from 4 MPa to 8 MPa.
- (3) However, CO₂ breakthrough occurs earlier at higher injection pressures.
- (4) The permeability heterogeneity in the reservoir is reduced after a threshold time (~500 days) although the overall heterogeneity is increased relative to the initial condition is overall increased for both non-CO₂ and CO₂ injection scenarios. This indicates that the homogenizing influence of CO₂-sorption-swelling is outpaced by CH₄-desorption-shrinkage and effective stress influences. This leaves the reservoir open to short-circuiting and earlier breakthrough of CO₂ rather than having this effect damped-out by the homogenizing influence of swelling.
- (5) The cumulative volume of CO₂ produced and stored in the reservoir is proportional to the injection pressure.

Acknowledgements

This work is a result of funding by ConocoPhillips. This support is gratefully acknowledged. We thank two anonymous reviewers for their insightful comments which improved the manuscript.

References

- [1] Karacan CÖ. Heterogeneous sorption and swelling in a confined and stressed coal during CO₂ injection. *Energy Fuels* 2003;17:1595–608.
- [2] Larsen JW. The effects of dissolved CO₂ on coal structure and properties. *Int J Coal Geol* 2004;57:63–70.
- [3] IPCC. Special report in carbon dioxide capture and storage. Cambridge; 2005.
- [4] Rogers RE. *Coalbed methane: principles and practice*. Englewood Cliffs, NJ: PTR Prentice Hall; 1994.
- [5] White CM, Smith DH, Jones KL, Goodman AL, Jikich SA, LaCount RB, et al. Sequestration of carbon dioxide in coal with enhanced coalbed methane recovery – a review. *Energy & Fuels* 2005;19:659–724.
- [6] Hall FE, Zhou C, Gasem KAM, Robinson RL, Jr., Yee D. 1994. Adsorption of pure methane, nitrogen, and carbon dioxide and their binary mixtures on Wet Fruitland coal, SPE Eastern Regional Meeting. Society of Petroleum Engineers, Charleston, West Virginia.
- [7] Krooss BM, van Bergen F, Gensterblum Y, Siemons N, Pagnier HJM, David P. High-pressure methane and carbon dioxide adsorption on dry and moisture-equilibrated Pennsylvanian coals. *Int J Coal Geol* 2002;51:69–92.
- [8] Harpalani S, Chen G. Estimation of changes in fracture porosity of coal with gas emission. *Fuel* 1995;74:1491–8.
- [9] Mavor MJ, Gunter WD. Secondary porosity and permeability of coal vs. gas composition and pressure. *Soc Petrol Eng Reservoir Eval Eng* 2006;114–25.
- [10] Kumar H, Elsworth D, Liu J, Pone D, Mathews JP. Optimizing enhanced coalbed methane recovery for unhindered production and CO₂ injectivity. *Int J Greenhouse Gas Control* 2012;11:86–97.
- [11] Harpalani S, Schraufnagel RA. Shrinkage of coal matrix with release of gas and its impact on permeability of coal. *Fuel* 1990;69:551–6.
- [12] Harpalani S, Chen G. Influence of gas production induced volumetric strain on permeability of coal. *Geotech Geol Eng* 1997;15:303–25.
- [13] Cui X, Bustin RM. Volumetric strain associated with methane desorption and its impact on coalbed gas production from deep coal seams. *AAPG Bull* 2005;89:1181–202.
- [14] Levine JR. Model study of the influence of matrix shrinkage on absolute permeability of coal bed reservoirs. *Geol Soc London Spec Publ* 1996;109:197–212.

- [15] Pone JDN, Halleck PM, Mathews JP. 3D characterization of coal strains induced by compression, carbon dioxide sorption, and desorption at in-situ stress conditions. *Int J Coal Geol* 2010;82:262–8.
- [16] Chikatamarla L, Cui X, Bustin RM. Implications of volumetric swelling/shrinkage of coal in sequestration of acid gases. In: International coalbed methane symposium proceedings, Tuscaloosa, AL; 2004.
- [17] Bustin RM, Cui X, Chikatamarla L. Impacts of volumetric strain on CO₂ sequestration in coals and enhanced CH₄ recovery. *AAPG Bull* 2008;92:15–29.
- [18] Pekot LJ, Reeves SR. Modeling the effects of matrix shrinkage and differential swelling on coalbed methane recovery and carbon sequestration. Department of Energy; 2002.
- [19] Chikatamarla L, Bustin RM, Cui X. CO₂ sequestration into coalbeds: insights from laboratory experiments and numerical modeling. *AAPG Stud Geol* 2009;59:457–74.
- [20] Shi JQ, Durucan S. A numerical simulation study of the Allison unit CO₂-ECBM pilot: the impact of matrix shrinkage and swelling on ECBM production and CO₂ injectivity. In: Rubin ES, Keith DW, Gilboy CF, Wilson M, Morris T, Gale J, Thambimuthu K, editors. 7th International conference on greenhouse gas control technologies; 2004.
- [21] Fokker PA, van der Meer LGH. The injectivity of coalbed CO₂ injection wells. *Energy* 2004;29:1423–9.
- [22] Mitra A, Harpalani S, Liu S. Laboratory measurement and modeling of coal permeability with continued methane production: Part 1 – laboratory results. *Fuel* 2012;94:110–6.
- [23] Wang GX, Wei XR, Wang K, Massarotto P, Rudolph V. Sorption-induced swelling/shrinkage and permeability of coal under stressed adsorption/desorption conditions. *Int J Coal Geol* 2010;83:46–54.
- [24] Shen J, Qin Y, Wang GX, Fu X, Wei C, Lei B. Relative permeabilities of gas and water for different rank coals. *Int J Coal Geol* 2011;86:266–75.
- [25] Day S, Duffy G, Sakurovs R, Weir S. Effect of coal properties on CO₂ sorption capacity under supercritical conditions. *Int J Greenhouse Gas Control* 2008;2:342–52.
- [26] Wang S. Gas transport, sorption, and mechanical response of fractured coal. In: Energy and mineral engineering. University Park: The Pennsylvania State University; 2012.
- [27] Viète DR, Ranjith PG. The effect of CO₂ on the geomechanical and permeability behaviour of brown coal: implications for coal seam CO₂ sequestration. *Int J Coal Geol* 2006;66:204–16.
- [28] Chen Z, Liu J, Elsworth D, Connell LD, Pan Z. Impact of CO₂ injection and differential deformation on CO₂ injectivity under in-situ stress conditions. *Int J Coal Geol* 2010;81:97–108.
- [29] Masoudian-Saadabad M, Airey D, Gainey A, Morris T, Berger J. The mechanical properties of CO₂-saturated coal specimens. In: Harmonising rock engineering and the environment. CRC Press; 2011.
- [30] Weniger P, Francú J, Hemza P, Krooss BM. Investigations on the methane and carbon dioxide sorption capacity of coals from the SW Upper Silesian Coal Basin, Czech Republic. *Int J Coal Geol* 2012;93:23–39.
- [31] Hol S, Peach CJ, Spiers CJ. Applied stress reduces the CO₂ sorption capacity of coal. *Int J Coal Geol* 2011;85:128–42.
- [32] Reeves SR. Enhanced CBM recovery, coalbed CO₂ sequestration assessed. *Oil Gas J* 2003;101:49.
- [33] Clarkson CR, Jordan CL, Gierhart RR, Seidle JP. Production data analysis of coalbed-methane wells. *SPE Reservoir Eval Eng* 2008;11:311–25.
- [34] Shi J-Q, Durucan S. Exponential growth in San Juan Basin Fruitland coalbed permeability with reservoir drawdown: model match and new insights. *SPE Reservoir Eval Eng* 2010;13:914–25.
- [35] Wu Y, Liu J, Chen Z, Elsworth D, Pone D. A dual poroelastic model for CO₂-enhanced coalbed methane recovery. *Int J Coal Geol* 2010;86:177–89.
- [36] Durucan S, Shi J-Q. Improving the CO₂ well injectivity and enhanced coalbed methane production performance in coal seams. *Int J Coal Geol* 2009;77:214–21.
- [37] Cui X, Bustin RM, Chikatamarla L. Adsorption-induced coal swelling and stress: implications for methane production and acid gas sequestration into coal seams. *J Geophys Res* 2007;112:B10202.
- [38] Liu J, Chen Z, Elsworth D, Miao X, Mao X. Linking gas-sorption induced changes in coal permeability to directional strains through a modulus reduction ratio. *Int J Coal Geol* 2010;83:21–30.
- [39] Bai M, Elsworth D, Roegiers JC. Modeling of naturally fractured reservoirs using deformation dependent flow mechanism. *International Journal of Rock Mechanics and Mining Sciences & Geomechanics Abstracts* 1993;30:1185–91.
- [40] Liu J, Chen Z, Elsworth D, Miao X, Mao X. Evaluation of stress-controlled coal swelling processes. *Int J Coal Geol* 2010;83:446–55.
- [41] Palmer I. Permeability changes in coal: analytical modeling. *Int J Coal Geol* 2009;77:119–26.
- [42] Palmer I, Mansoori J. How permeability depends on stress and pore pressure in coalbeds: a new model. In: SPE annual technical conference and exhibition, society of petroleum engineers, Denver, Colorado; 1998.
- [43] Pan Z, Connell LD, Camilleri M, Connelly L. Effects of matrix moisture on gas diffusion and flow in coal. *Fuel* 2010;89:3207–17.
- [44] Shi J-Q, Durucan S. A model for changes in coalbed permeability during primary and enhanced methane recovery. *SPE Reservoir Eval Eng* 2005;8:291–9.
- [45] Shi J-Q, Durucan S. Modelling of mixed-gas adsorption and diffusion in coalbed reservoirs. In: SPE unconventional reservoirs conference, Keystone, Colorado, USA; 2008.
- [46] Clarkson CR, Pan Z, Palmer I, Harpalani S. Predicting sorption-induced strain and permeability increase with depletion for coalbed-methane reservoirs. *SPE J* 2010;15:152–9.
- [47] Gu F, Chalaturnyk RJ. Numerical simulation of stress and strain due to gas sorption/desorption and their effects on in situ permeability of coalbeds. *J Can Pet Technol* 2006;45:52–62.
- [48] Ouyang Z, Elsworth D. Evaluation of groundwater flow into mined panels. *Int J Rock Mech Min Sci Geomech Abstr* 1993;30:71–9.
- [49] Liu J, Elsworth D, Brady BH. Analytical evaluation of post-excavation hydraulic conductivity field around a tunnel. *Int J Rock Mech Min Sci* 1997;34:181.e181–187.
- [50] Wu Y, Liu J, Elsworth D, Siriwardane H, Miao X. Evolution of coal permeability: contribution of heterogeneous swelling processes. *Int J Coal Geol* 2011;88:152–62.
- [51] Fujioka M, Yamaguchi S, Nako M. CO₂-ECBM field tests in the Ishikari Coal Basin of Japan. *Int J Coal Geol* 2010;82:287–98.
- [52] Wu Y, Liu J, Elsworth D, Chen Z, Connell L, Pan Z. Dual poroelastic response of a coal seam to CO₂ injection. *Int J Greenhouse Gas Control* 2010;4:668–78.
- [53] Tao S, Wang Y, Tang D, Xu H, Lv Y, He W, et al. Dynamic variation effects of coal permeability during the coalbed methane development process in the Qinshui Basin, China. *Int J Coal Geol* 2012;93:16–22.
- [54] Rice DD. Composition and origins of coalbed gas; 1993.
- [55] Langmuir I. The constitution and fundamental properties of solids and liquids. Part I: solids. *J Am Chem Soc* 1916;38:2221–95.
- [56] Ertekin T, King GA, Schwerer FC. Dynamic gas slippage: a unique dual-mechanism approach to the flow of gas in tight formations.
- [57] Mora CA, Wattenbarger RA. Analysis and verification of dual porosity and CBM shape factor. *J Can Pet Technol* 2009;48.
- [58] Warren JE, Root PJ. The behavior of naturally fractured reservoirs. *SPE J* 1963;3:245–55.
- [59] Liu J, Wang J, Chen Z, Wang S, Elsworth D, Jiang Y. Impact of transition from local swelling to macro swelling on the evolution of coal permeability. *Int J Coal Geol* 2011;88:31–40.
- [60] Saffman PG, Taylor G. The penetration of a fluid into a porous medium or Hele-Shaw cell containing a more viscous liquid. *Proc R Soc London Ser A Math Phys Sci* 1958;245:312–29.
- [61] Wong S, Macdonald D, Andrei S, Gunter WD, Deng X, Law D, et al. Conceptual economics of full scale enhanced coalbed methane production and CO₂ storage in anthracitic coals at South Qinshui basin, Shanxi, China. *Int J Coal Geol* 2010;82:280–6.
- [62] Wong S, Law D, Deng X, Robinson J, Kadatz B, Gunter WD, et al. Enhanced coalbed methane and CO₂ storage in anthracitic coals—micro-pilot test at South Qinshui, Shanxi, China. *Int J Greenhouse Gas Control* 2007;1:215–22.
- [63] NIST. Thermophysical properties of fluid systems. <<http://webbook.nist.gov/chemistry/fluid/>>.
- [64] Mavor MJ, Gunter WD, Robinson JR. Alberta multiwell micro-pilot testing for CBM properties, enhanced methane recovery and CO₂ storage potential. Society of Petroleum Engineers; 2004.
- [65] Reeves S, Taillefert A, Pekot L, Clarkson C. The Allison unit CO₂-ECBM pilot: a reservoir modeling study. U.S. Department of Energy; 2003.
- [66] Gunter B, Wong S, Law D, Sanli F, Jianping Y, Zhiqiang F. Enhanced coalbed methane (ECBM) field test at South Qinshui Basin, Shanxi Province, China. In: GCEP workshop. Beijing: Alberta Research Council; 2005.